Quaternary Science Reviews 207 (2019) 37–48

Contents lists available at ScienceDirect

Quaternary Science Reviews

journal homepage: www.elsevier.com/locate/quascirev

Erosion rates in Fennoscandia during the past million years

J.D. Jansen [a, *], M.F. Knudsen [a], J.L. Andersen [a, b], J. Heyman [c], D.L. Egholm [a]

[a] Department of Geoscience, Aarhus University, 8000, Aarhus, Denmark
[b] Geological Survey of Norway, 7491, Trondheim, Norway
[c] Department of Earth Sciences, University of Gothenburg, 40530, Göteborg, Sweden

ARTICLE INFO

Article history:
Received 6 December 2018
Received in revised form
16 January 2019
Accepted 16 January 2019

Keywords:
Bedrock glacial erosion
Markov chain Monte Carlo inversion
Cosmogenic nuclide memory
Scandinavia

ABSTRACT

The widespread existence of cosmogenic nuclides accumulated in bedrock prior to the last glaciation demonstrates the limited erosional efficacy of the most recent Fennoscandian and Laurentide ice sheets. Yet the deeper history of erosion in these landscapes repeatedly blanketed by ice remains essentially unknown. Here we present the first comprehensive ice sheet-wide analysis of cosmogenic ^{10}Be data ($n = 953$) from the Fennoscandian landscape. We find 64% of all sampled bedrock surfaces contain ^{10}Be inheritance, including >85% of blockfields and tors, and >50% of ice-carved terrain, in addition to 27% of ice-transported boulders. Recent ice sheets scoured landscapes well beyond glacial troughs and nuclide inventories reveal a patchy legacy of erosional effectiveness that diminishes at high elevations, such that 89% ($n = 55$) of bedrock samples retain inheritance above 1600 m. We exploit this widespread nuclide inheritance in a Markov chain Monte Carlo-based inversion model to estimate long-term erosion rates and surface exposure histories from 113 paired ^{10}Be–^{26}Al bedrock samples. Nuclide inventories with or without inheritance convey equally important information about the erosional effectiveness of the last ice sheet. We define *cosmogenic nuclide memory* as the residence time of bedrock samples inside the nuclide-production window ($\leq$2 m depth) where ~80% of the total nuclide production occurs. The cosmogenic nuclide memory is set by mean erosion rate and varies from ~10 ka for samples eroded >2 m during the last glaciation to > 1-Ma for the slowest erosion rates. We find that mean erosion rates are well constrained compared to the ratio of exposure to burial. The inclusion of bedrock erosion in our computations thwarts the capacity to constrain surface exposure history or identify former nunataks from paired ^{10}Be–^{26}Al data. Ice-carved surfaces reflect diverse erosion histories that are not straightforward to interpret from surficial morphology alone. Relative to the ~10 mm/kyr benchmark for polar ice masses, we report point-based mean erosion rates that vary by more than three orders of magnitude, with glacial troughs and areal-scour terrain eroding at ~1 to >100 mm/kyr, blockfields at 0.8–16 mm/kyr, and tors at 0.8–7.7 mm/kyr (5th–95th percentiles).

1. Introduction

Glacial troughs and areally-scoured terrain extend over vast areas repeatedly covered by the northern hemisphere ice sheets, yet the history of erosion here is essentially unknown beyond the last glaciation (Sugden and John, 1976). Because glacier beds remain largely inaccessible, insights to subglacial erosion processes rely heavily upon interpretations of landscapes exposed by ice retreat. Along high-latitude continental margins, troughs cut 1–3 km deep by ice are commonly interspersed by high plateaus with undulating surfaces marked by variable responses to overriding ice, which range from areal scouring to largely unmodified regolith mantles. Subglacial erosion rates are known to differ greatly over short distances and perhaps even decrease by 1–2 orders of magnitude over a single glacial cycle (Kleman and Glasser, 2007; Koppes and Montgomery, 2009; Fernandez et al., 2011). This time dependence confounds estimates of recent glacial erosion (Hallet et al., 1996; Koppes et al., 2015) since high proglacial sediment yields are potentially transient signals of recent glacial retreat and are not representative of landscape-forming processes over Quaternary timescales (Koppes and Montgomery, 2009; Fernandez et al., 2011). Across Laurentide and Fennoscandian landscapes the imprint of the last ice sheet is widely observed, yet the palimpsest of preceding glaciations has proved difficult to clarify (Sugden, 1978; White,

* Corresponding author.
E-mail address: jdj@geo.au.dk (J.D. Jansen).

https://doi.org/10.1016/j.quascirev.2019.01.010

1988; Kleman and Stroeven, 1997; Kleman et al., 2008). Glacial erosion can be successfully quantified over 10^5–10^6-yr timescales with low-temperature thermochronometry (Reiners and Brandon, 2006), but this method cannot resolve the shorter timescales associated with < 1-km spatial patterns of erosion that are distinctive of glaciated landscapes and it is often less effective on the slowly exhumed passive continental margins (Nielsen et al., 2009; Medvedev and Hartz, 2015) that comprise most of Earth's formerly ice-covered terrain.

Exposure dating with cosmogenic nuclides has transformed knowledge of glacial erosion and past ice sheets (Nishiizumi et al., 1991; Briner and Swanson, 1998; Fabel et al., 2002; Jansen et al., 2014). Cosmogenic nuclides, such as ^{10}Be and ^{26}Al, accumulate in minerals within a few metres of Earth's surface as a function of exposure to secondary cosmic rays and are lost via erosion and radionuclide decay (Lal, 1991; Gosse and Phillips, 2001). Since most of the cosmogenic inventory is removed by 2 m of bedrock erosion, nuclide abundances in bedrock reveal the erosional effectiveness of the last ice sheet. Minimal erosion has the effect of preserving nuclides inherited from previous ice-free intervals and is indicated by cosmogenic nuclide abundances that exceed postglacial production. Burial beneath an ice sheet halts nuclide production, while radionuclide decay reduces abundances and the ^{26}Al/^{10}Be ratio specifically. Nuclide inheritance and the ^{26}Al/^{10}Be ratio, therefore, hold information about the depth of subglacial erosion and the history of ice cover and surface exposure prior to the last ice sheet (Nishiizumi et al., 1991; Briner and Swanson, 1998; Fabel et al., 2002; Briner et al., 2006; Margreth et al., 2016; Strunk et al., 2017).

Here, we examine the distribution of inheritance in the Fennoscandian landscape based on a comprehensive compilation of ^{10}Be measurements ($n = 953$). We then apply a Markov chain Monte Carlo-based inversion model (Knudsen et al., 2015) to paired ^{10}Be–^{26}Al data ($n = 113$) from bedrock landforms spanning the area buried repeatedly by Fennoscandian Ice Sheets. We attempt to constrain the history of surface erosion and exposure on a wide range of glacial troughs, areally-scoured terrain, blockfields, and tors. We find that mean erosion rates vary by more than three orders of magnitude while retaining systematic trends between bedrock landform types.

2. Topographic legacy of glaciation in Fennoscandia

The topographic imprint of recurrent glacial and interglacial periods was pursued early in Fennoscandia (Richter, 1896; Reusch, 1910). A notable lack of erosion by the last ice sheet was described by Ahlmann (1919) and the erosional legacy of multiple glaciations has been debated over the century since. The persistence of preglacial landscapes drew the attention of early workers, especially the interpretation of high elevation, low-relief terrain known as palaeic surfaces (e.g., Reusch, 1901; Ahlmann, 1919; Rudberg, 1954). Analogous arguments were proposed for Baffin Island (Sugden and Watts, 1977; Andrews et al., 1985) and Greenland (Sugden, 1974) and subsequent work (e.g., Kleman, 1994; Lidmar-Bergström, 1996; Kleman and Stroeven, 1997; Japsen et al., 2018) fitted easily with the contention that multiple glaciations in Fennoscandia left a limited erosional imprint aside from deepening valley troughs and inserting fjords at the continental margin. The existence of preglacial landforms, despite overriding ice, was attributed to the development of frozen-bed patches at high elevations, which preserve the underlying surfaces from erosion (Sugden, 1974; Sugden and John, 1976).

Applications of cosmogenic analyses have bolstered these largely qualitative ideas by showing that extensive areas in the Scandinavian mountains contain ^{10}Be–^{26}Al inventories that accumulated prior to burial under the last ice sheet (Brook et al., 1996; Fabel et al., 2002; Stroeven et al., 2002). More recently, improved understanding of ice dynamics and the emergence of glacial and periglacial landscape evolution models (Anderson, 2002, Andersen et al., 2015; Egholm et al., 2015, 2017) have sparked a series of challenges to previous ideas regarding the genesis of high elevation, low-relief terrain and the topographic legacy of glaciation (Nielsen et al., 2009; Steer et al., 2012; Egholm et al., 2017). Two long-standing questions are key to addressing these conflicting views: 1) What is the spatial distribution and depth of glacial erosion in the Scandinavian mountains? and 2) Are preglacial materials likely to exist at high elevations? We address these questions by quantifying long-term erosion rates and exposure histories on a range of bedrock landforms distributed across the Scandinavian mountains, including glacial troughs, areally-scoured terrain, blockfields and tors (Fig. 1).

U-shaped glacial troughs are classic indicators of valley deepening by glacial ice. According to the model of selective linear erosion (Sugden, 1974; Sugden and John, 1976), glacial troughs are progressively deepened beneath thick ice at the pressure-melting point while intertrough areas are preserved under frozen-bed, weakly erosive ice. Consistent with this model, an elevation-dependent relationship in cosmogenic nuclide abundances is widely observed (Li et al., 2005; Briner et al., 2006; Strunk et al., 2017; Andersen et al., 2018). Based on topographic reconstructions, up to ~2 km of fjord incision has occurred along the Scandinavian west coast whereas the larger glacial valleys east of the ridgepole have probably incised <400 m, though locally as deep as 900 m (Fredin, 2002; Stroeven et al., 2002; Kleman and Stroeven, 1997).

Areal scour is a general description of glacial plucking and abrasion guided by patterns of bedrock jointing and fracture, which yields a rugged array of streamlined bedrock, stoss-lee forms, and rock basins, all with typically <100 m of relief (Sugden and John, 1976). Fast basal sliding and possibly even ice streams (Krabbendam and Bradwell, 2014) are thought to be responsible for areal scour observed at elevations spanning lowlands to plateaus and summits. The total depth of glacial erosion associated with areal scour is the subject of a long debate (Krabbendam and Bradwell, 2014) with suggestions ranging from <50 m (Sugden, 1978) to 100–150 m (White, 1988).

Blockfields (felsenmeer) and tors are central to arguments about the efficacy of glacial erosion and survival of preglacial forms (Sugden and Watts, 1977; Kleman and Stroeven, 1997; Fabel et al., 2002; Ballantyne, 1998, 2010; Goodfellow, 2007). The blockfields dealt with here are autochthonous veneers of coarse regolith in a fine-grained matrix draping smoothly convex summits on the intertrough plateaus (Goodfellow, 2007). Since they are incompatible with basal sliding and they are thought to develop over multiple glacial cycles, the distribution of blockfields and tors is used to infer patterns of frozen-bed ice over the last glacial cycle (Kleman and Stroeven, 1997; Briner et al., 2006; Margreth et al., 2016). Many blockfields show signs of glacial modification and in some cases areal scouring may have removed them completely (Kleman et al., 2008). In the absence of direct dating, the presence of chemical or physical weathering products in blockfield mantles is often the basis for inferring formation under either warm preglacial (Strømsøe and Paasche, 2011) or cold late Cenozoic (Goodfellow, 2012) climates, respectively. Blockfields may otherwise contain elements of both (Ballantyne, 2010), but testing this possibility requires knowledge of long-term erosion rates—our objective here.

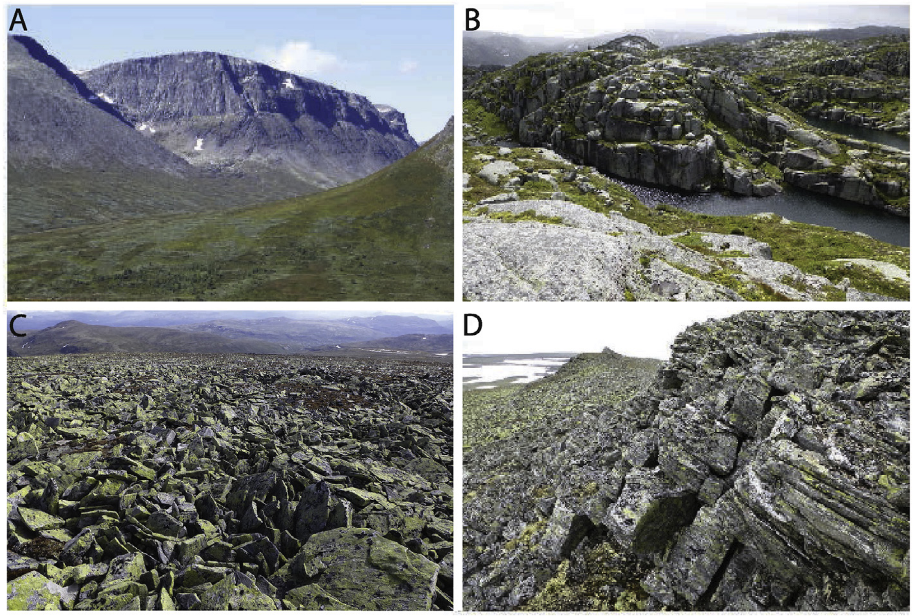

Fig. 1. Bedrock landforms overridden by the Fennoscandian Ice Sheet: A) Glacial trough shows ~850 m relief, Smådaladn, Norway. B) Areally-scoured terrain with <150 m relief, plucked and abraded surfaces, and sparse regolith, south of Lysefjorden, Norway. C) Blockfield mantling a parabolic summit crest, Reinheimen, Norway. D) Tor with open joints and rubbly outcrop, Reinheimen. Note the absence of signs of recent glacial erosion on the blockfield and tor.

3. Methods

3.1. Mapping ^{10}Be inheritance and landform classification

We compile 953 cosmogenic ^{10}Be measurements on bedrock and ice-transported boulders from sites inside the maximum extent of the Fennoscandian Ice Sheet during the Last Glacial Maximum (Supplementary Table S1). All cosmogenic nuclide data are standardised and recalculated using the online calculators formerly known as the CRONUS-Earth online calculators (Balco et al., 2008) v. 2.3 with St (Stone, 2000) time-constant production rate scaling and reference production rates of 4.09 ± 0.22 atoms/g/yr (^{10}Be) and 27.97 ± 2.65 atoms/g/yr (^{26}Al), based on the expage-201702 calibration dataset and methods (see http://expage.github.io/production). All computations assume a ^{10}Be half-life of 1.387 Myr (Chmeleff et al., 2010; Korschinek et al., 2010) and ^{26}Al half-life of 0.705 Myr (Nishiizumi, 2004).

The presence of a significant level of nuclides inherited from prior to the last ice sheet is indicated by ^{10}Be apparent exposure ages ($\pm 1\sigma$, external uncertainty) that exceed local deglaciation ages per Stroeven et al. (2016) to which we apply an uncertainty of $\pm$500 yr (Supplementary Table S1). This uncertainty is a conservative estimate of the maximum likely deviation of post-Younger Dryas (<11.5 kyr) ice-margin positions. Our ^{10}Be dataset includes 363 bedrock samples and 590 samples from ice-transported (glacial erratic) boulders. We classify the bedrock samples into one of four landform classes based primarily on surface morphology (Fig. 1): glacial trough, areal scour, blockfield, and tor. We apply these terms following the descriptions given by authors in the original publications together with our own assessment of online aerial photograph resources (www.norgeibilder.no, www.kartor.eniro.se) and *Google Earth* imagery. We define glacial troughs ($n = 56$) broadly as kilometre-scale linear structures of positive topographic curvature (i.e., concave-up). While recognising that not all Scandinavian mountain valleys show advanced glacial modification, all were buried repeatedly by Pleistocene ice sheets and almost all those sampled pertain to 'glacial valleys'. Our areal-scour class ($n = 209$) is applied in a similar unrestrictive sense to mean largely exposed bedrock terrain, often lake-scattered, with kilometre-scale negative topographic curvature (i.e., convex-up). Areally-scoured terrain is typically found at mid to high elevations on the intertrough plateaus, but a handful of low-elevation sites are also included. Areal scour and blockfields ($n = 84$) share the same negative-curvature intertrough terrain, but areal scour is marked by glacial erosion whereas blockfields constitute more or less continuous cover of autochthonous regolith derived from local bedrock (i.e., we regard these as bedrock samples). Tors ($n = 14$) are not landscape-scale forms but we include them in our scheme because they provide key insights to the efficacy of glacial erosion. They typically occur as knolls of in situ bedrock standing above autochthonous blockfields or transported glacigenic materials.

Given that the samples in our dataset were collected and analysed to address diverse research questions, we expect some systematic bias. Sample selection often favours less eroded topographic crests to minimise snow shielding, and paired ^{10}Be–^{26}Al measurements often follow an anticipated surface inheritance. Such a bias would lead to underestimating broadscale erosion rates. On the other hand, studies seeking to establish exposure ages may have sought fresher-looking outcrops, though paired ^{10}Be–^{26}Al data are not routinely measured in such cases.

3.2. Markov chain Monte Carlo-based inversion model

To constrain surface erosion rates in Fennoscandia, we apply the Markov chain Monte Carlo-based (MCMC) inversion model of Knudsen et al. (2015) to paired ^{10}Be–^{26}Al data from bedrock ($n = 113$, a subset of our larger compilation, Fig. 2 and Supplementary Table S2). This approach entails a system of forward models that compute iteratively the ^{10}Be and ^{26}Al concentrations in surface bedrock due to exposure, burial, and erosion over glacial and interglacial periods. The predicted final nuclide concentrations are compared to the measured concentrations, thereby mapping a range of landscape evolution scenarios compatible with the ^{10}Be–^{26}Al data available. It is a key assumption of this model that

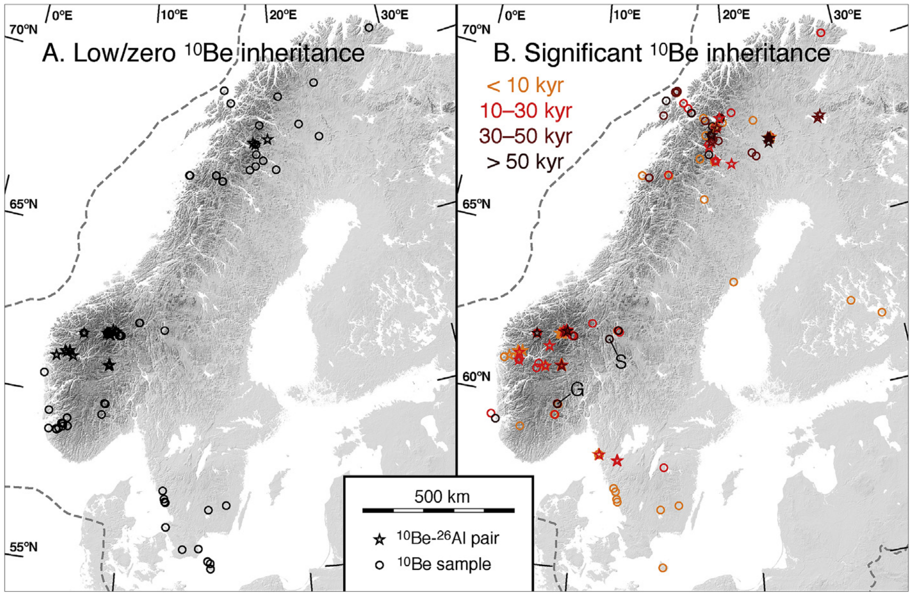

Fig. 2. Fennoscandia hillshade digital elevation map showing the geographical distribution of our compiled bedrock cosmogenic ^{10}Be data (n = 363) from inside the LGM extent of the Fennoscandian Ice Sheet (grey dashes, Stroeven et al., 2016): A) Bedrock samples with low/zero ^{10}Be inheritance (n = 131) defined as ^{10}Be apparent exposure age (±1σ) less than or overlapping with deglaciation age (±500 yr). B) Bedrock samples with significant inheritance (n = 232) defined as ^{10}Be apparent exposure age (±1σ) exceeding deglaciation age (±500 yr) and shown in four colour-keyed bins of inheritance: < 10 kyr, 10–30 kyr, 30–50 kyr, and >50 kyr. High mountain sites, Sølen (S) and Gaustatoppen (G), are shown and discussed in the main text. Note three far-flung samples in NW Russia are not shown. (For interpretation of the references to colour in this figure legend, the reader is referred to the Web version of this article.)

the exposure/burial history at a site can be subdivided into two distinct regimes: 1) ice-covered intervals characterised by subglacial erosion and no cosmogenic nuclide production due to shielding by the overlying ice mass, and 2) ice-free intervals characterised by subaerial erosion and continuous exposure. We assume no significant shielding occurs due to snow, till, or vegetation throughout these ice-free intervals. Erosion rates associated with the ice-covered and ice-free regimes are independent and vary from sample to sample, but at a given sampling point, two constant erosion rates are ascribed to the two regimes, respectively. This assumption simplifies the Quaternary erosion history to a piecewise combination of two erosion rates: one for glacial periods and one for interglacial periods. This simplified two-stage erosion model allows the MCMC inversion to constrain erosion rates in many cases, but it may not apply where, for example, the thermal configuration of an ice sheet shifts from warm-based to cold-based (or vice versa) over time. We discuss this limitation below.

Our approach builds upon the concept introduced by Fabel et al. (2002) in which a δ^{18}O-threshold value is applied to a global benthic δ^{18}O record representing past changes in global ice volume. For our simulations, a randomly selected δ^{18}O threshold value between 3.2 and 4.9 (Lisiecki and Raymo, 2005) serves to define ice-covered versus ice-free intervals. The δ^{18}O record is smoothed using a 5-kyr running-mean such that major marine isotope stages and sub-stages are captured and being consistent with what is known of large-scale glacial advances and retreats in Fennoscandia (Fabel et al., 2002; Mangerud et al., 2011). For each sample, the last glacial-interglacial transition is defined by the site-specific deglacial age of Stroeven et al. (2016) to which we assign an uncertainty of ±500 yr. We apply the same nuclide production rates, scaling schemes, and half-lives, as those noted above including attenuation lengths and updated elevation-dependant muon cross-sections implemented in v. 2.3 of the former CRONUS-Earth online calculators (Balco et al., 2008).

To conduct a thorough search of the model space, we use four MCMC walkers and accept 50,000 simulations per walker—the ratio of accepted to rejected models is 0.4 (after Knudsen et al., 2015). The performance of the walkers is monitored as the simulations unfold by tracking the acceptance ratios and the residuals (computed as weighted least-squares) between simulated and measured data. If one walker performs significantly worse than others, it is omitted from further analyses. The simulations associated with each walker are then combined into a total ensemble of accepted simulations for each sample (~200,000 in most cases), which is then used to define the range of likely δ^{18}O threshold values. The most likely erosion history of each sample is computed from the three free model parameters (i.e., δ^{18}O threshold, glacial and interglacial erosion rate). Mean erosion rate is the product of glacial and interglacial erosion rates that are constant through time and is computed from the average depth of the sample at 1-Ma (Knudsen et al., 2015). We use the 5, 25, 50, 75, and 95th percentiles to define the spectra of most likely model outputs, including mean erosion rate, total cumulative exposure time, and δ^{18}O threshold value.

The MCMC model simulates the full 2.6 Myr of the Quaternary period, but the timescale over which cosmogenic nuclides resolve erosion rate varies with the erosion rate itself for each sample. Considering the depth dependence of cosmogenic nuclide production, we define the *cosmogenic nuclide memory* as the time that eroding material spends inside the nuclide-production window. We set the base of this window at 2 m depth, above which ~80% of the total depth-integrated nuclide production (for bedrock) takes place. This is a longer-term extension of the integration timescale that is based upon the absorption depth scale for production by spallation (Lal, 1991). We prefer the 2 m production window because muonic production below the absorption depth is relatively important for samples with inheritance.

4. Results

4.1. Cosmogenic nuclide inheritance

Inheritance is mainly a function of the erosional effectiveness of the last ice sheet. We find that 73% of ice-transported boulders and 36% of bedrock surface samples contain low or zero ^{10}Be inheritance (i.e., ^{10}Be apparent exposure age [± 1σ] is less than or overlaps with deglaciation age [± 500 yr]) meaning these sites probably experienced > 2 m of erosion during the last glaciation (Figs. 3 and 4). Hence, most ice-transported boulders yield exposure ages that match, or are younger than, deglaciation (Heyman et al., 2011). The remaining 27% of boulders and 64% of bedrock surfaces contain significant ^{10}Be inheritance (i.e., ^{10}Be apparent exposure age [± 1σ] exceeds deglaciation age [± 500 yr]). Blockfields and tors show the highest frequency of significant inheritance: 89% of blockfield samples and 86% of tor samples, yet even here cases of low inheritance occur due to erosion by the last ice sheet. For the ice-carved glacial troughs and areal-scour sites, the inheritance frequency distributions are notably similar (Fig. 4A), with significant inheritance retained in 52% of glacial trough and 56% of areal-scour bedrock samples.

At high elevations we find many blockfields and areal-scour sites with high levels of inheritance (Fig. 4B), suggesting an overall lack of erosion by the last ice sheet: 89% of all bedrock samples above 1600 m contain significant ^{10}Be inheritance (Fig. 4B). Conversely, samples with low/zero inheritance are more abundant at lower elevations, due to erosion by the last ice sheet (Fig. 4C).

4.2. Inversion model outputs

A set of two-nuclide plots grouped according to the four landform classes provides an overview of the ^{10}Be–^{26}Al dataset (Fig. 5). Our MCMC-based inversion model can constrain mean erosion rates for 72 of the 113 paired ^{10}Be–^{26}Al samples. The remaining 41 sample pairs contain low/zero inheritance and pertain to sites scoured during the last glaciation; for these we can estimate only

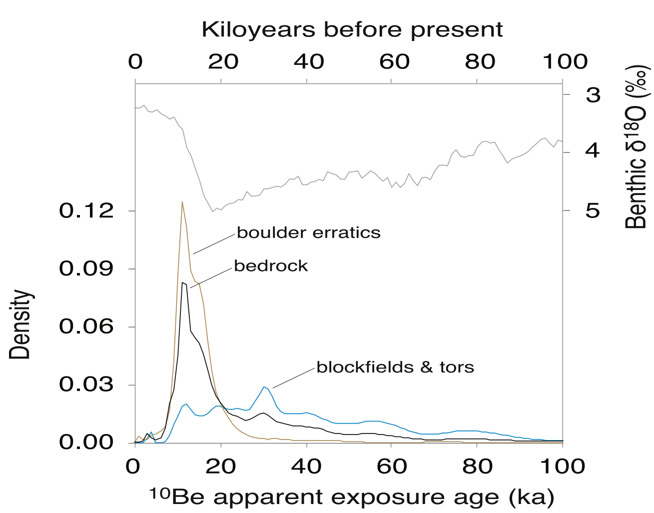

Fig. 3. Kernel density estimates of ^{10}Be apparent exposure ages computed for samples of glacial boulder erratics (n = 590), blockfields and tors (n = 98), and bedrock landforms (n = 363, inclusive of blockfields and tors). Kernel density estimates are averaged Gaussian curves representing each exposure age, using 1-kyr bandwidth. Axes on right and top (and grey line) shows benthic δ^{18}O data (Lisiecki and Raymo, 2005), which is a proxy for global ice volume. Modal peaks in the frequency of ^{10}Be ages from boulders and bedrock correspond to the timing of the last deglaciation across central Fennoscandia ~12–10 ka (matching the δ^{18}O data). Blockfields and tors show a stronger tendency for nuclide inheritance.

minimum erosion rates integrated within the last glacial cycle (Fig. 6A). Bedrock erosion rate is broadly an inverse function of apparent exposure age following the steady-state relationship described by Lal (1991, Eq. (14)). This steady-state relationship assumes continuous exposure and does not account for intervals of burial beneath ice. In Fig. 6A, samples with low/zero inheritance can be seen extending above the steady-state curve, hence for these we can constrain only minimum erosion rate. The smear of models below the steady-state curve is the product of intervals of ice cover and zero nuclide production. Total nuclide production declines as the duration of ice-cover grows and therefore models with exceptionally slow erosion go hand in hand with low cumulative exposure times. Samples with slow erosion and lengthy burial retain a long cosmogenic nuclide memory, because their nuclide inventory accumulated while moving slowly through the 2 m nuclide-production window (Fig. 6B).

A cohort of samples yields extremely low erosion rates (<1 mm/kyr) coupled with low cumulative exposure times and δ^{18}O thresholds. These sample pairs with ^{26}Al/^{10}Be ratios ≤5.4 plot along the base of Fig. 7A and show as outliers in the two-nuclide plots (Fig. 5). The generally high nuclide abundance and low ^{26}Al/^{10}Be ratios of these samples force the MCMC model to compute a high proportion of burial (>90% at P_{50} [i.e., 50th percentile], see Supplementary Table S2 for a summary of MCMC outputs of mean erosion rate, exposure time, and δ^{18}O threshold). Such long burial is implausible given the associated δ^{18}O thresholds (<3.5) are within the bounds of current interglacial levels (Lisiecki and Raymo, 2005) and glaciers cover only ~ 5% of the mountains today. The explanation for these results could be either: 1) erroneous ^{26}Al measurements, which is plausible given that many are from the early (pre-2000) phase of the cosmogenic nuclide method, or 2) our inversion-model assumption of constant glacial and interglacial erosion rates does not apply (Knudsen and Egholm, 2018). We return to this limitation below.

Bedrock mean erosion rates plotted against elevation reveal a cluster of well constrained, slowly-eroding blockfields and areal scour at elevations above about 1500 m (Fig. 8). Tors exhibit uniformly slow erosion. At mid-elevations of ~600–1500 m glacial troughs and areal-scour samples yield widely varying erosion rates, from slow to fast, and many with unconstrained upper limits.

With the aim of comparing erosion rate patterns between landforms, we aggregate the erosion rate data into normalised frequency histograms based on all ~22.6 million accepted MCMC models from the 113 sample pairs (Fig. 9). Ice-carved surfaces in glacial troughs and areal-scour sites erode at ~1 to >100 mm/kyr (P_{5-95}) and display heavy-tailed frequency distributions that include a component of unconstrained upper erosion-rate limits. The blockfields and tors, by comparison, have much narrower distributions (Fig. 9). Blockfields are shaped by periglacial processes involving frost-driven sediment production and diffusional sediment transport at erosion rates of ~0.8–16 mm/kyr (P_{5-95}). Tors, too, are currently subject to rock disintegration via the action of frost and insolation at somewhat slower rates of ~0.8–7.7 mm/kyr (P_{5-95}).

Surface exposure-burial history (Fig. 7) is notably less well constrained compared to mean erosion rate, although it broadly compares with previous modelling attempts based on δ^{18}O data (Kleman and Stroeven, 1997; Fabel et al., 2002; Kleman et al., 2008). There is no apparent trend with elevation (Fig. 7B) nor identifiable differences between the mountain sites and lowland tors, though the latter were probably not covered by mountain-centred ice sheets.

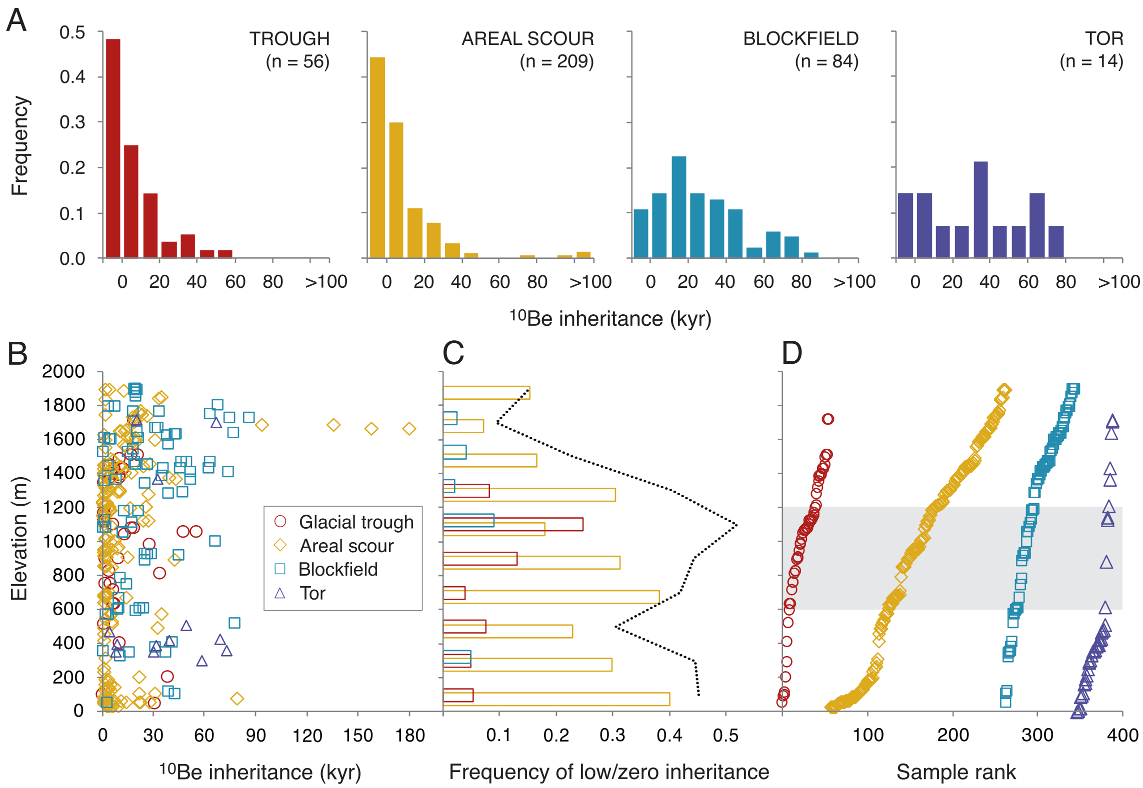

Fig. 4. A) Frequency histograms of ^{10}Be inheritance (kyr) per landform, where inheritance is ^{10}Be apparent exposure age minus deglaciation age and frequency is normalised by the number of samples; note non-linear *x*-axes and samples with low/zero inheritance are shown in bins to the left of 0-kyr. Overall, 36% of bedrock samples were eroded >2 m by the last ice sheet, leaving the rest with significant inheritance. B) Scatterplot of bedrock ^{10}Be inheritance (kyr) versus elevation for samples with significant inheritance (n = 232); age uncertainties are omitted. C) Histograms showing frequency distribution of ^{10}Be bedrock samples with low/zero inheritance per 200 m elevation bins (n = 129, excluding 2 tor samples for clarity). Frequencies are normalised by dividing the number of eroded samples by the total count per elevation bin; summed frequencies are shown as black dashes, and histogram colours match legend in B. The distribution indicates how >2 m erosion by the last ice sheet varies weakly with elevation, although erosion is restricted at elevations above 1600 m where inheritance is preserved in 89% of all bedrock samples. D) Rank plot of elevation distribution of all bedrock samples; symbols match legend in B. Tors in our dataset (n = 14) are supplemented by observations (n = 30) from undated tors (André, 2002; Olesen et al., 2012), highlighting that tors are rarely observed between ~600 and 1200 m (grey band), though other sampled landforms are fairly evenly distributed with elevation. (For interpretation of the references to colour in this figure legend, the reader is referred to the Web version of this article.)

5. Discussion

5.1. Validity of the inversion model

Inversion modelling has not been widely applied to cosmogenic nuclide data, unlike thermochronometry where it forms the core of analyses (e.g., Reiners and Brandon, 2006). The MCMC-based approach is especially well-suited to settings in which ice masses sporadically interrupt nuclide production, yet we accept that our two-stage erosion assumption (two different rates of glacial and interglacial erosion) is unlikely to hold strictly for those bedrock surfaces subject to episodic glacial quarrying. Samples of this kind may be among the cohort showing extreme levels of burial (Figs. 5 and 7). A long recognised pitfall with interpreting exposure-burial history from ^{10}Be–^{26}Al data arises from the inability to discriminate long-term burial from episodic acceleration in erosion rate (Gosse and Phillips, 2001; Knudsen and Egholm, 2018). One means of simplifying the problem has been to fix erosion rate to zero (preferably backed by field observations) and to compute minimum exposure histories. This approach worked well for the early appraisals of glacial landscapes (e.g., Nishiizumi et al., 1991; Bierman et al., 1999; Fabel et al., 2002); however, more recent variations (e.g., Beel et al., 2016; Corbett et al., 2016) tend to downplay glacial erosion to an extent that may be unjustified (cf. Egholm et al., 2017). Despite the appealing simplicity of neglecting erosion in computations, our results demonstrate that inclusion of non-zero erosion causes potential exposure histories to proliferate wildly (Fig. 7), leaving little prospect of reconstructing the long-term ratio of exposure to burial. Our approach successfully estimates erosion rates (Figs. 6 and 8), provided one permits the constraining influence of the two-stage erosion-rate assumption applied to glacial and interglacial intervals; the MCMC model strives to balance the number of free parameters (3) with constraints provided by observations. As noted by Knudsen et al. (2015), accounting explicitly for non-steady erosion rates during glacial periods would render the problem intractable unless additional nuclides are measured from depth profiles. Such data are not yet available on the scale presented here, but pairing ^{10}Be with nuclides of much shorter half-life, such ^{36}Cl or ^{14}C, offers greater chronometric sensitivity (e.g., Briner et al., 2014).

5.2. Surficial morphology and the temporal evolution of erosion rates

The elevation-dependence of nuclide inheritance observed in some studies (e.g., Li et al., 2005; Briner et al., 2006; Strunk et al., 2017; Andersen et al., 2018) disappears in our ice-sheet wide compilation. Spatial patterns of ^{10}Be inheritance do not show overall elevation-dependence, although the erosional efficiency of the last ice sheet decreases sharply at high elevations and 89% of all bedrock samples above 1600 m contain significant ^{10}Be inheritance (Fig. 4B). Recent Fennoscandian ice sheets scoured bedrock across

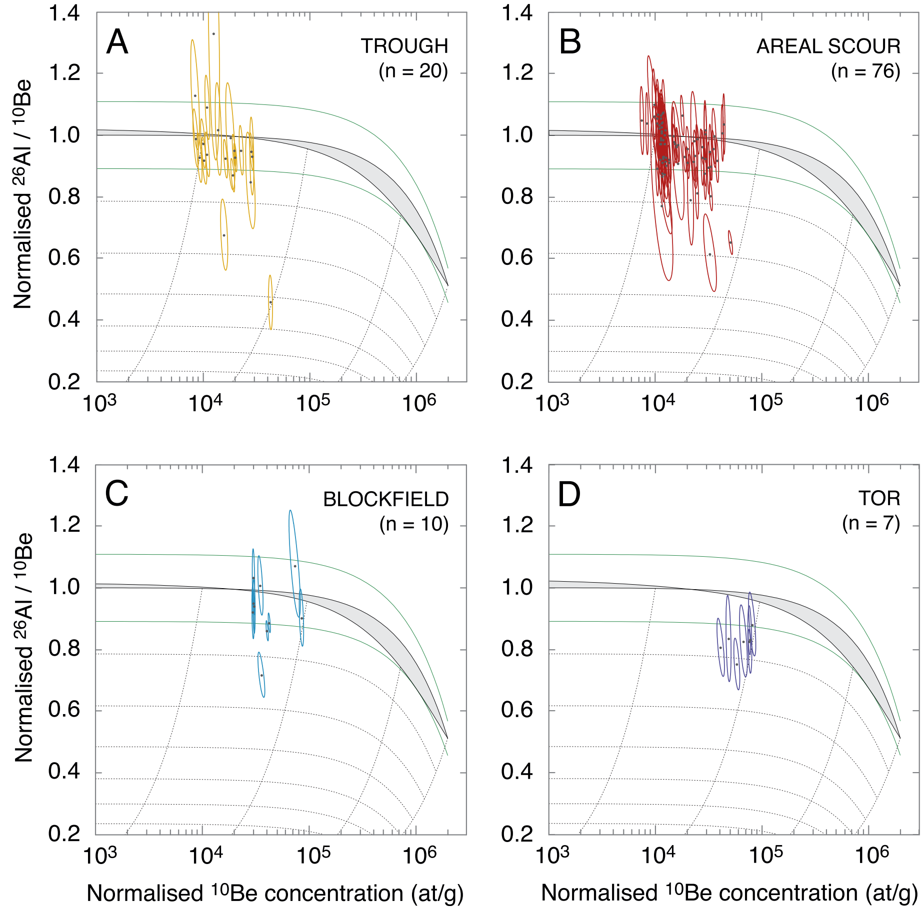

Fig. 5. Two-nuclide plots of all paired ^{10}Be–^{26}Al data (n = 113) for Fennoscandia normalised to the ^{10}Be reference production rate (4.09 ± 0.22 at/g/yr) and ^{26}Al reference production rate (27.97 ± 2.65 at/g/yr). Shown are uncertainties (±1 σ) in ^{10}Be and ^{26}Al concentrations (coloured ellipses); uncertainties in the apparent exposure line based on $^{26}Al/^{10}Be$ production rate uncertainties (green lines) (see http://expage.github.io/production); and the steady-state erosion island (grey fill). A) glacial trough (n = 20), B) areal scour (n = 76), C) blockfield (n = 10), and D) tor (n = 7). (For interpretation of the references to colour in this figure legend, the reader is referred to the Web version of this article.)

the mid-elevations that span intertrough plateaus, including the 11% of blockfield samples with low/zero inheritance (Fig. 4A,C). Low/zero inheritance is also present among 44% of areal scour samples (Fig. 4A,C) and it is conceivable from their setting that these bare bedrock areas have hosted blockfields in the past. The glacial scouring is not necessarily recent, as shown by the significant inheritance contained within the remaining 56% of areal scour sites, including the four oldest ^{10}Be apparent exposure ages in our dataset (i.e., ~103–190 ka at Sølen: SO99-4, –5, –8, and –9) (Figs. 2 and 4A,B, Supplementary Table S1). Conversely, we note some blockfields in our dataset, such as those at Gaustatoppen (Linge et al., 2006, Supplementary Table S1), display shallow rock basins suggestive of glacial erosion at some time in the past. Strong similarities exist among the erosion-rate frequency distributions of the ice-carved landforms (Fig. 9), despite their contrasting surficial morphology and spatial positioning in the landscape. As with areal-scour sites, we find an unexpectedly high proportion (52%) of glacial troughs were not eroded substantially during the last glaciation.

Two plausible explanations can account for these findings: 1) erosive and non-erosive ice masses have tended to exist in the same place at different times, possibly even within the same glacial cycle (Kleman and Glasser, 2007; Koppes and Montgomery, 2009); and 2) topographic evolution of continental margins, especially fjord incision, has caused shifts in ice-sheet dynamics resulting in systematic variations that favour erosion along some valleys and not others (Kessler et al. 2008; Refsnider and Miller, 2010, 2013; Egholm et al., 2017). Both points relate to the task of integrating glacial erosion rates over different timescales and we expand on that below.

5.3. Timescales of erosion

With the aim to quantify bedrock erosion beyond the last glaciation, thermochronometry and onshore-offshore mass balance analyses have been applied widely to Fennoscandia. Good support exists for a broad-scale average exhumation rate of <10 mm/kyr since the late Palaeozoic (Medvedev and Hartz, 2015), but the details and timing of km-scale exhumation remain disputed (e.g., Nielsen et al., 2009; Chalmers et al., 2010). Rates of mass transfer offshore from western Scandinavia indicate accelerated erosion linked to late Pliocene-Pleistocene glaciation (since ~ 2.7–2.8 Myr). Spatially-averaged erosion rates for the mountain source area are estimated at ~190 mm/kyr (Dowdeswell et al., 2010) and ~130 mm/kyr (Steer et al., 2012), and for southern Fennoscandia ~150 mm/kyr since 1.1 Myr (Hjelstuen et al., 2012)—although these and other such records are subject to imprecise source area constraints and/or chronometric control (Anell et al., 2010; Hall et al., 2013).

As exhumation advects material upwards, cosmogenic nuclides record the residence time of bedrock samples in the nuclide-production window (<2 m depth). This residence time, or cosmogenic nuclide memory, records the surface processes that led to

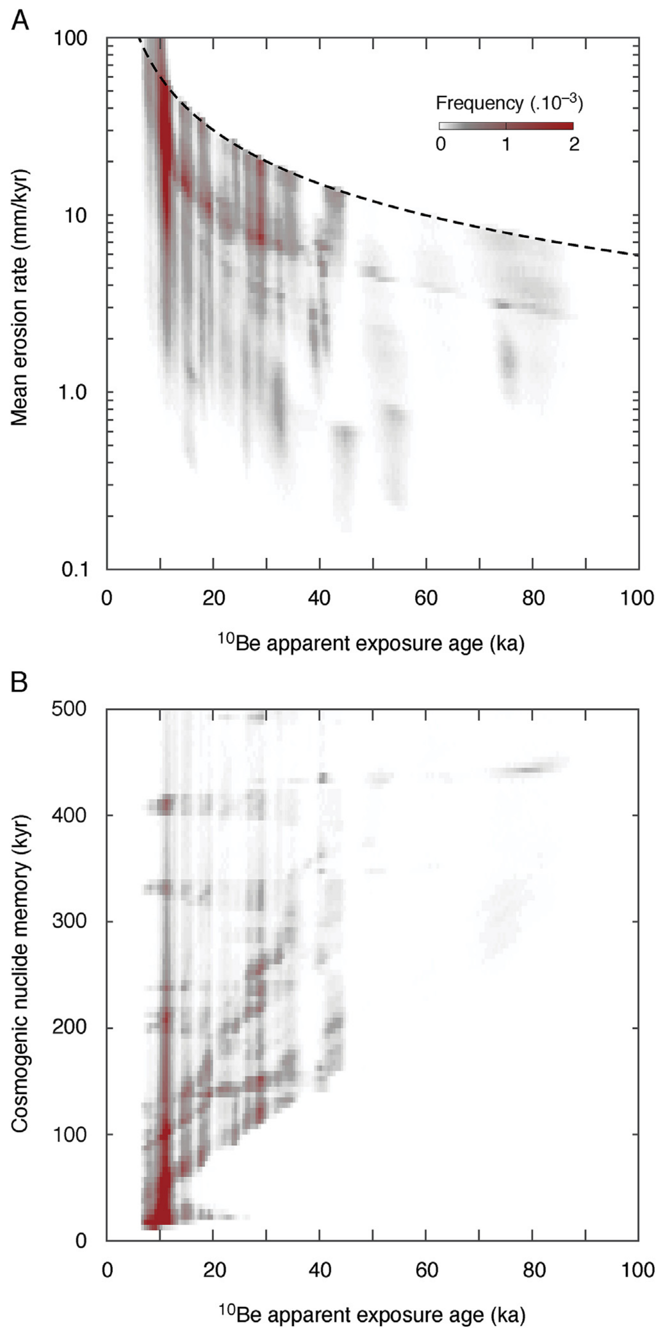

Fig. 6. Two-dimensional frequency histograms, with a graduated colour bar showing full frequency distributions of accepted MCMC models for each sample (~22.6 million in total). A) Mean bedrock erosion rate versus ^{10}Be apparent exposure age (paired ^{10}Be–^{26}Al data, n = 113). The dashed curve indicates steady-state erosion assuming continuous exposure (Lal, 1991, Eq. (14)). Samples (models) with low ^{10}Be age (~10 ka) and therefore low/zero inheritance, can be seen extending above the steady-state curve; for these samples we can delimit only minimum erosion rates. For the remaining samples (^{10}Be age > 10 ka), mean erosion rates fall under the dashed curve due to the influence of periods of ice-cover and zero nuclide production. B) Cosmogenic nuclide memory versus ^{10}Be apparent exposure age (paired ^{10}Be–^{26}Al data, n = 113). Nuclide memory is the residence time of a bedrock sample once it enters the nuclide-production window, which we define as 2 m depth, where ~80% of the total nuclide production occurs. (For interpretation of the references to colour in this figure legend, the reader is referred to the Web version of this article.)

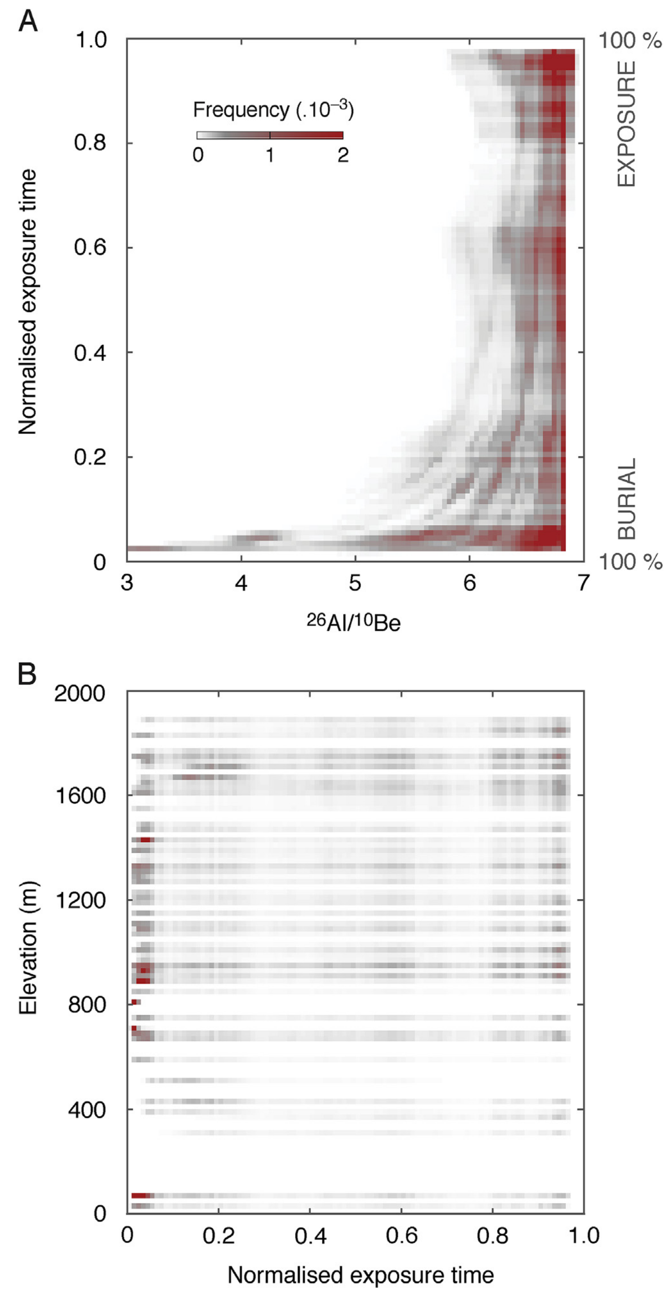

Fig. 7. Two-dimensional frequency histograms. A) Normalised exposure time versus ^{26}Al/^{10}Be ratio (n = 113), defined as the fraction of time in which samples were producing cosmogenic nuclides unshielded by ice. B) Elevation versus normalised exposure time. For both plots, the graduated colour bar shows the full frequency distributions of accepted MCMC models for each sample (~22.6 million in total). Both plots reveal that inclusion of bedrock erosion in the computations disables reconstructions of exposure history. Note the samples with exceptionally low cumulative exposure times mostly reflect a cohort (^{26}Al/^{10}Be ratios ≤ 5.4) described in the main text. (For interpretation of the references to colour in this figure legend, the reader is referred to the Web version of this article.)

removal of the upper 2 m of bedrock, and in our Fennoscandian dataset varies from ~10 ka for samples eroded >2 m during the last glaciation to > 1-Ma for the slowest erosion rates (Fig. 6B) (Supplementary Table S2). Nuclide memory has clear merits for sites that are exposed discontinuously; it simultaneously conveys mean erosion rate while accounting for the majority (~80%) of the total depth-integrated nuclide production.

Our mean bedrock erosion rates span more than three orders of magnitude <1.0 to >100 mm/kyr. Modern erosion rates in Norway based on proglacial sediment yields from 15 glaciers range from 60 to 960 mm/kyr (unweighted mean ~ 330 mm/kyr) (Hallet et al.,

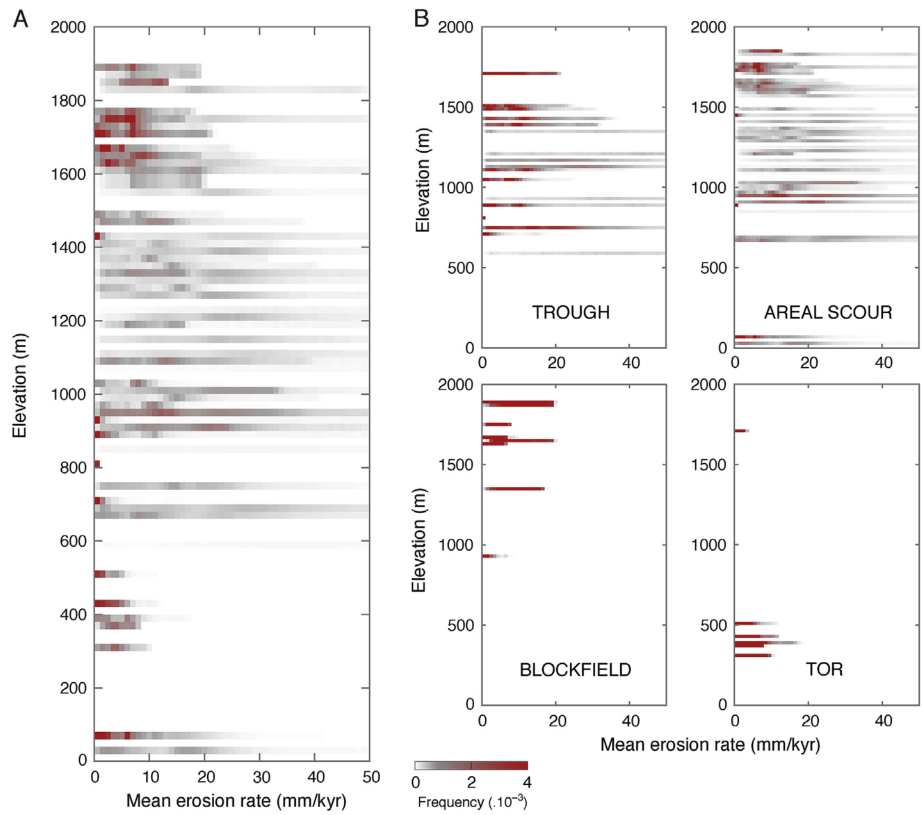

Fig. 8. A) Two-dimensional frequency histogram of mean bedrock erosion rate versus elevation (paired ^{10}Be–^{26}Al data, n = 113). Graduated colour bar shows full distributions of accepted MCMC models for each sample (~22.6 million in total). Upper erosion-rate limits are unconstrained for samples with low ^{10}Be age due to insufficient information (inheritance), as shown by grey bands extending > 50 mm/kyr. B) Same data as shown in A) per four landform classes: glacial trough (n = 20), areal scour (n = 76) blockfield (n = 10), and tor (n = 7). (For interpretation of the references to colour in this figure legend, the reader is referred to the Web version of this article.)

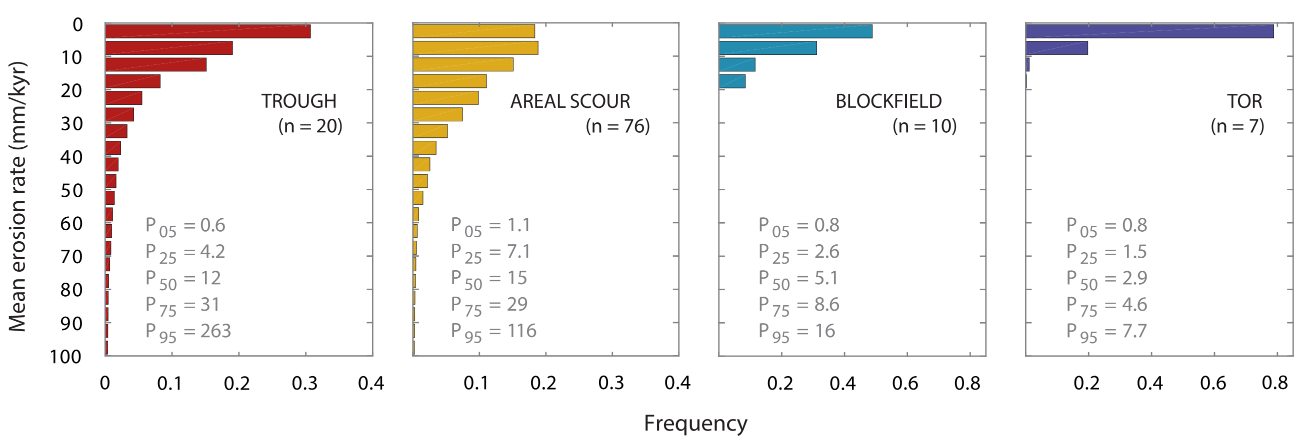

Fig. 9. Frequency histograms of mean erosion rates per bedrock landform. Frequencies are the aggregated sum of ~22.6 million accepted MCMC models for the four landforms (paired ^{10}Be–^{26}Al data, n = 113) normalised by the number of samples; note the scales on the *x*-axes differ. Erosion rate percentiles (P with subscript) in mm/kyr are listed in each.

1996), which is overall faster than our long-term erosion rates, although recall that for 36% of our sample pairs (those with low/zero inheritance) we can constrain minimum erosion rates only. Basin-wide subglacial erosion rates are reported to vary ~10^1–10^5 mm/kyr globally, while those at polar latitudes are generally restricted to <100 mm/kyr (Hallet et al., 1996; Koppes and Montgomery, 2009). Yet, the conventional view that polar ice masses erode slowly has shifted in light of basin-wide erosion rates of 1000–1800 mm/kyr from west Greenland averaged over the historical period (Young et al., 2016). Relative to the ~10 mm/kyr benchmark for polar ice masses (Hallet et al., 1996), we find point-specific long-term erosion can be an order of magnitude slower (<1 mm/kyr), and potentially much faster (>100 mm/kyr) in glacial troughs and areally-scoured terrain (Figs. 6 and 9). These findings highlight the spatial dimension of subglacial erosion rate variations and when considered alongside variations that arise due to shifting subglacial thermal conditions over a single glacial cycle (Kleman and Glasser, 2007; Koppes et al., 2009; 2015), it seems inevitable that bedrock erosion will be fundamentally patchy.

Another explanation for wide variations in glacial erosion rates may relate to the long-term topographic evolution of the continental margin and its effects on ice dynamics. A striking contrast in the Scandinavian mountains exists between glacial troughs and many intertrough plateau areas that display few or no signs of glacial erosion (as noted also for Baffin Island, e.g., Sugden and Watts, 1977; Briner et al., 2006, 2014). A key question concerns whether the latter areas have always hosted non-erosive, cold-based ice and, if not, what caused the subglacial thermal organisation to change? Glacial transformation of these former fluvial landscapes and especially the insertion of fjords over multiple glaciations heralded new ice dynamics and associated erosion patterns, as shown by computational modelling (Kessler et al., 2008; Egholm et al., 2017). Isostatic uplift associated with erosional unloading in fjords raised the intertrough plateaus and funnelled progressively more ice into fjords, leaving thin, non-erosive ice at high elevations—some of which support blockfields today (Egholm et al., 2017). Attendant shift over time in the selective incision of some troughs in preference to others is one possible explanation for the inheritance preserved in more than half of the ice-carved landforms in our dataset (Fig. 4). Nevertheless, the mismatch between surficial appearances and recent bedrock erosion rate implies patterns of glacial erosion have not been constant in space nor in time and hence recent glacial cycles are unlikely to be representative of the earliest Fennoscandian glaciations (Fabel et al., 2002; Egholm et al., 2017). For this reason, we advocate caution when extrapolating field observations of glacial erosion and preservation patterns beyond 1-Myr.

5.4. Implications for previous views of the Fennoscandian landscape

Rates of lowering along glacial troughs have been unquestionably fast. For instance, the estimated 400–900 m of valley incision in northern Sweden (Kleman and Stroeven, 1997; Fredin, 2002; Stroeven et al., 2002) amounts to ~150–350 mm/kyr of incision averaged over the Quaternary, while ~2000–2850 m of incision along Sognefjorden in southern Norway yields ~800–1100 mm/kyr (Nesje et al., 1992). The so-called palaeic relief distributed across the intertrough plateaus has long been viewed as preserving erosional remnants of an uplifted preglacial landscape that has experienced minimal glacial erosion (Reusch, 1901; Ahlmann, 1919; Rudberg, 1954; Lidmar-Bergström, 1996; Japsen et al., 2018). Yet, the persistence of preglacial mountain landforms throughout the late Cenozoic glaciations has never been corroborated with geochronometry. Our study is the first systematic assessment of bedrock landform erosion rates over 10^3–10^6 yr timescales across the Scandinavian mountains from the coast and inland (Fig. 2).

The intertrough blockfields comprise a thin blanket of regolith formed by long-term processes of physical and chemical weathering (Ballantyne, 1998, 2010; Goodfellow, 2007, 2012; Strømsøe and Paasche, 2011). Accordingly, we find mean erosion rates range ~0.8–16 mm/kyr (P_{5-95}) yet, especially in western Norway, intertrough areas were extensively scoured by the last ice sheet and 44% of areal-scour sites in our compilation experienced > 2 m of erosion. Such erosion seems incompatible with broadscale preservation of preglacial surfaces. More problematic is the practice of ascribing ages to erosional terrain and the inevitable judgement regarding the amount of surface lowering permitted for such a surface to be still identifiable. All exposed bedrock surfaces are eroding—some fast, some slow—but rates of more than a few mm/kyr demand improbably thick preglacial regolith for any such material to be preserved today on the mountain plateaus. This is not to say that ancient materials do not exist in Scandinavia; they undeniably do, as shown by Triassic K–Ar ages on clay-rich saprolites (i.e. highly weathered in situ bedrock) at three low-elevation sites in the south (Fredin et al., 2017). But the precise relationship between these saprolites and a Mesozoic landsurface remains ambiguous and, while many other clay-rich saprolites are reported (Olesen et al., 2012), so far none has been found at elevations > 600 m.

Fragile bedrock tors in Scandinavia and elsewhere indicate minimal glacial erosion, corresponding to frozen-bed patches beneath ice sheets (Stroeven et al., 2002; Paasche et al., 2006). Most tors in our dataset are located on the Baltic Shield, although a few occur at high elevations in the mountains. Given that tors are common in non-glaciated granitic terrain, it seems likely that they were developed over much wider areas in Scandinavia up until the late Cenozoic glaciations, including the slowly eroding mountains where weathering processes may have predominated for many millions of years (Nielsen et al., 2009). Combining the cosmogenic-dated tors presented here (n = 14) with another set of observations from undated tors (n = 1 from André, 2002; n = 29 from Olesen et al., 2012) we note tors rarely occur between ~600 and 1200 m (Fig. 4D). This 'tor gap', albeit crudely defined, is consistent with the destruction of blockfields and tors by sliding ice — along with the absence of clay-rich saprolites — across an elevation interval matching that of the most intense glacial erosion (Figs. 4C and 8).

6. Conclusions

We have conducted an ice sheet-wide analysis of cosmogenic nuclide data (^{10}Be and ^{26}Al) from the Fennoscandian landscape with the aim to investigate the extent and depth of erosion. A spatial framework of landforms guides our MCMC-based inversion approach to constraining erosion rates integrated over timespans ranging from the last deglaciation (~10 ka) to the past 1-Myr. Our main conclusions are summarised as follows.

1) Recent ice sheets scoured landscapes well beyond glacial troughs and nuclide inventories reveal a patchy legacy of erosional effectiveness. By comparing 363 bedrock ^{10}Be apparent exposure ages with a deglaciation chronology (Stroeven et al., 2016), we find that 64% of bedrock surfaces contain ^{10}Be inheritance, including > 85% of blockfields and tors, and >50% of ice-carved terrain (glacial troughs and areal scour) (Figs. 4 and 9). A similar comparison of 590 ice-transported boulders reveals 27% with ^{10}Be inheritance. The distribution of nuclide inheritance is mainly a function of the erosional effectiveness of the last ice sheet, which diminishes at high elevations such that ^{10}Be inheritance is retained in 89% of bedrock samples above 1600 m (Figs. 4 and 8). While nuclide inheritance is widely distributed in the Scandinavian mountains, we note the absence of exceptionally old (>200 ka) exposure ages (Fig. 4B) relative to those reported from other North Atlantic margins, Baffin Island (Briner et al., 2006; Margreth et al., 2016) and Greenland (Beel et al., 2016).
2) We develop the idea of *cosmogenic nuclide memory*: the residence time of bedrock samples inside the nuclide-production window within 2 m of the surface where ~80% of the total nuclide production occurs (Fig. 6B). This differs from the integration timescale that is based upon the absorption depth scale for production by spallation (Lal, 1991). Cosmogenic nuclide memory is set by the mean erosion rate and in our Fennoscandian dataset varies from ~10 ka for samples eroded >2 m during the last glaciation to > 1-Myr for the slowest erosion rates.
3) Bedrock mean erosion rates vary by more than three orders of magnitude. Relative to the benchmark erosion rate of ~10 mm/kyr for polar ice masses (Hallet et al., 1996), point-specific long-term erosion in Fennoscandia can be an order of magnitude

slower (<1 mm/kyr) or potentially much faster (>100 mm/kyr) in glacial troughs and areally-scoured terrain (Figs. 4 and 9). Such wide variation in erosion rates blurs the distinction that is often made between polar and temperate ice masses in terms of ice dynamics, subglacial thermal organisation, and erosion rates.

4) While glacial troughs and areal-scour surfaces are shown to have a diverse range of potential erosion histories (Fig. 9), their erosion-rate frequency distributions are similar despite having contrary positive (troughs) and negative (areal scour) curvature topography. This suggests that the surficial morphology of glaciated landscapes is often a poor indicator of long-term erosion history.
5) Intertrough plateau landscapes host rates of erosion that can be locally fast: 44% of areal scour sites and 11% of blockfields were eroded >2 m by the last ice sheet (Fig. 4A). We find mean erosion rates on areally-scoured terrain of ~1.1–116 mm/kyr (P_{5-95}), with blockfields eroding more slowly overall at ~0.8–16 mm/kyr (P_{5-95}). We recognise the large uncertainties involved with extrapolating such rates from intertrough areas over > 1-Myr timescales; nevertheless, our results imply that so-called palaeic relief on the plateaus is unlikely to preserve identifiable surfaces or even appreciable material predating late Cenozoic cooling, since ~15 Ma (Zachos et al., 2001). The intertrough plateau landscapes have dynamically evolved over recent glaciations via glacial and periglacial processes (Goodfellow, 2007, 2012; Egholm et al., 2015; Andersen et al., 2018), hence the commonly applied terms 'palaeic' and 'relict' are neither accurate nor useful. Instead, we advocate quantifying the rates at which these areas are eroding via observable and measurable surface processes.
6) Cosmogenic ^{10}Be and ^{26}Al inventories cannot discriminate ice shielding from subglacial erosion without additional independent constraints from field observations (Gosse and Phillips, 2001). Consequently, inclusion of erosion in computations effectively disables the capacity to resolve surface exposure histories (Figs. 5 and 7) or identify former nunataks from paired ^{10}Be–^{26}Al data. Neglecting bedrock erosion when reconstructing the exposure-burial history of ice-carved landscapes runs a high risk of error. The way forward is to make better use of more sensitive, shorter half-life nuclides such as ^{36}Cl and ^{14}C.

Acknowledgements

We acknowledge funding from the Danish Council for Independent Research (grant DFF-6108-00226) and Aarhus University Research Foundation to DLE. JDJ was also supported by a Marie Skłodowska-Curie Fellowship at the University of Potsdam. We thank Annina Margreth for a thorough and constructive review.

Appendix A. Supplementary data

Supplementary data to this article can be found online at https://doi.org/10.1016/j.quascirev.2019.01.010.

References

Ahlmann, H.W., 1919. Geomorphological studies in Norway. Geogr. Ann. 1, 1–148.
André, M.-F., 2002. Geomorphic evidence for recurrent cold-based ice conditions in Nordic uplands during the Quaternary glaciations (Aurivaara Plateau, North Sweden). Nor. J. Geogr. 56, 74–79.
Andersen, J.L., Egholm, D.L., Knudsen, M.F., Jansen, J.D., Nielsen, S.B., 2015. The periglacial engine of mountain erosion – Part 1: rates of frost cracking and frost creep. Earth Surface Dynamics 3, 447–462.
Andersen, J.L., Egholm, D.L., Knudsen, M.F., Linge, H., Jansen, J.D., Pedersen, V.K., Nielsen, S.B., Tikhomirov, D., Olsen, J., Fabel, D., Xu, S., 2018. Widespread erosion on high plateaus during recent glaciations in Scandinavia. Nat. Commun. 9, 830.
Anderson, R.S., 2002. Modeling the tor-dotted crests, bedrock edges, and parabolic profiles of high alpine surfaces of the Wind River Range, Wyoming. Geomorphology 46, 35–58.
Andrews, J.T., Stravers, J.A., Miller, G.H., 1985. Patterns of glacial erosion and deposition around Cumberland Sound, Frobisher Bay and Hudson Strait, and the location of ice streams in the eastern Canadian Arctic. In: Woldenburg, M.J. (Ed.), Models in Geomorphology. Allen and Unwin, London, pp. 93–117.
Anell, I., Thybo, H., Stratford, W., 2010. Relating Cenozoic North Sea sediments to topography in southern Norway: the interplay between tectonics and climate. Earth Planet. Sci. Lett. 300, 19–32.
Balco, G., Stone, J.O., Lifton, N., Dunai, T.J., 2008. A complete and easily accessible means of calculating surface exposure ages or erosion rates from ^{10}Be and ^{26}Al measurements. Quat. Geochronol. 3, 174–195.
Ballantyne, C.K., 1998. Age and significance of mountain-top detritus. Permafr. Periglac. Process. 9, 327–345.
Ballantyne, C.K., 2010. A general model of autochthonous blockfield evolution. Permafr. Periglac. Process. 21, 289–300.
Beel, C.R., Lifton, N.A., Briner, J.P., Goehring, B.M., 2016. Quaternary evolution and ice sheet history of contrasting landscapes in Uummannaq and Sukkertoppen, western Greenland. Quat. Sci. Rev. 149, 248–258.
Bierman, P.R., Marsella, K.A., Patterson, C., Davis, P.T., Caffee, M., 1999. Mid-Pleistocene cosmogenic minimum-age limits for pre-Wisconsinan glacial surfaces in southwestern Minnesota and southern Baffin Island: a multiple nuclide approach. Geomorphology 27, 25–39.
Briner, J.P., Swanson, T.W., 1998. Using inherited cosmogenic ^{36}Cl to constrain glacial erosion rates of the Cordilleran ice sheet. Geology 26, 3–6.
Briner, J.P., Lifton, N.A., Miller, G.H., Refsnider, K., Anderson, R., Finkel, R., 2014. Using in situ cosmogenic ^{10}Be, ^{14}C, and ^{26}Al to decipher the history of polythermal ice sheets on Baffin Island, Arctic Canada. Quaternary Geochronolology 19, 4–13.
Briner, J.P., Miller, G.H., Thompson Davis, P., Finkel, R.C., 2006. Cosmogenic radionuclides from fiord landscapes support differential erosion by overriding ice sheets. Geol. Soc. Am. Bull. 118, 406–420.
Brook, E.J., Nesje, A., Lehman, S.J., Raisbeck, G.M., Yiou, F., 1996. Cosmogenic nuclide exposure ages along a vertical transect in western Norway: implications for the height of the Fennoscandian ice sheet. Geology 24, 207–210.
Chalmers, J.A., Green, P.F., Japsen, P., Rasmussen, E.S., 2010. The Scandinavian mountains have not persisted since the Caledonian orogeny. A comment on Nielsen et al. (2009). J. Geodyn. 50, 94–101.
Chmeleff, J., von Blanckenburg, F., Kossert, K., Jakob, D., 2010. Determination of the ^{10}Be half-life by multicollector ICP-MS and liquid scintillation counting. Nucl. Instrum. Methods Phys. Res. B 268, 192–199.
Corbett, L.B., Bierman, P.R., Rood, D.H., 2016. Constraining multi-stage exposure-burial scenarios for boulders preserved beneath cold-based glacial ice in Thule, northwest Greenland. Earth Planet. Sci. Lett. 440, 147–157.
Dowdeswell, J.A., Ottesen, D., Rise, L., 2010. Rates of sediment delivery from the Fennoscandian Ice Sheet through an ice age. Geology 8, 3–6.
Egholm, D.L., Andersen, J.L., Knudsen, M.F., Jansen, J.D., Nielsen, S.B., 2015. The periglacial engine of mountain erosion – Part 2: modelling large-scale landscape evolution. Earth Surface Dynamics 3, 463–482.
Egholm, D.L., Jansen, J.D., Brædstrup, C.F., Pedersen, V.K., Andersen, J.L., Ugelvig, S.V., Larsen, N.K., Knudsen, M.F., 2017. Formation of plateau landscapes on glaciated continental margins. Nat. Geosci. 10, 592–597.
Fabel, D., Stroeven, A.P., Harbor, J., Kleman, J., Elmore, D., Fink, D., 2002. Landscape preservation under Fennoscandian ice sheets determined from in situ produced ^{10}Be and ^{26}Al. Earth Planet. Sci. Lett. 201, 397–406.
Fernandez, R.A., Anderson, J.B., Wellner, J.S., Hallet, B., 2011. Timescale dependence of glacial erosion rates: a case study of Marinelli Glacier, Cordillera Darwin, southern Patagonia. J. Geophys. Res. 116, F01020.
Fredin, O., 2002. Glacial inception and Quaternary mountain glaciations in Fennoscandia. Quat. Int. 95–96, 99–112.
Fredin, O., Viola, G., Zwingmann, H., Sørlie, R., Brönner, M., Lie, J.-E., Grandal, E.M., Müller, A., Margreth, A., Vogt, C., Knies, J., 2017. The inheritance of a Mesozoic landscape in western Scandinavia. Nat. Commun. 14878.
Goodfellow, B.W., 2007. Relict non-glacial surfaces in formerly glaciated landscapes. Earth Sci. Rev. 80, 47–73.
Goodfellow, B.W., 2012. A granulometry and secondary mineral fingerprint of chemical weathering in periglacial landscapes and its application to blockfield origins. Quat. Sci. Rev. 57, 121–135.
Gosse, J.C., Phillips, F.M., 2001. Terrestrial in situ cosmogenic nuclides: theory and application. Quat. Sci. Rev. 20, 1475–1560.
Hall, A.M., Ebert, K., Kleman, J., Nesje, A., Ottesen, D., 2013. Selective glacial erosion on the Norwegian passive margin. Geology 41, 1203–1206.
Hallet, B., Hunter, L., Bogen, J., 1996. Rates of erosion and sediment evacuation by glaciers: a review of field data and their implications. Glob. Planet. Chang. 12, 213–235.
Heyman, J., Stroeven, A.P., Harbor, J.M., Caffee, M.W., 2011. Too young or too old: evaluating cosmogenic exposure dating based on an analysis of compiled boulder exposure ages. Earth Planet. Sci. Lett. 302, 71–80.
Hjelstuen, B.O., Nygård, A., Sejrup, H.P., Haflidason, H., 2012. Quaternary denudation of southern Fennoscandia—evidence from the marine realm. Boreas 41, 379–390.
Jansen, J.D., Codilean, A.T., Stroeven, A.P., Fabel, D., Hättestrand, C., Kleman, J., Harbor, J.M., Heyman, J., Kubik, P.W., Xu, S., 2014. Inner gorges cut by subglacial meltwater during Fennoscandian ice sheet decay. Nat. Commun. 5, 3815.
Japsen, P., Green, P.F., Chalmers, J.A., Bonow, J.M., 2018. Mountains of southernmost Norway: uplifted Miocene peneplains and re-exposed Mesozoic surfaces.

J. Geol. Soc. 175, 721–741.
Kessler, M.A., Anderson, R.S., Briner, J.P., 2008. Fjord insertion into continental margins driven by topographic steering of ice. Nat. Geosci. 1, 365–369.
Kleman, J., 1994. Preservation of landforms under ice sheets and ice caps. Geomorphology 9, 19–32.
Kleman, J., Glasser, N.F., 2007. The subglacial thermal organisation (STO) of ice sheets. Quat. Sci. Rev. 26, 585–597.
Kleman, J., Stroeven, A.P., 1997. Preglacial surface remnants and Quaternary glacial regimes in northwestern Sweden. Geomorphology 19, 35–54.
Kleman, J., Stroeven, A.P., Lundqvist, J., 2008. Patterns and Quaternary ice sheet erosion and deposition in Fennoscandia and a theoretical framework for explanation. Geomorphology 97, 73–90.
Knudsen, M.F., Egholm, D.L., 2018. Constraining Quaternary ice covers and erosion rates using cosmogenic ^{26}Al/^{10}Be nuclide concentrations. Quat. Sci. Rev. 181, 65–75.
Knudsen, M.F., Egholm, D.L., Jacobsen, B.H., Larsen, N.K., Jansen, J.D., Andersen, J.L., Linge, H.C., 2015. A multi-nuclide approach to constrain landscape evolution and past erosion rates in previously glaciated terrains. Quat. Geochronol. 30, 100–113.
Koppes, M., Montgomery, D., 2009. The relative efficacy of fluvial and glacial erosion over modern to orogenic timescales. Nat. Geosci. 2, 644–647.
Koppes, M., Hallet, B., Rignot, E., Mouginot, J., Smith Wellner, J., Boldt, K., 2015. Observed latitudinal variations in erosion as a function of glacier dynamics. Nature 526, 100103.
Korschinek, G., Bergmaierb, A., Faestermanna, T., Gerstmannc, U.C., Kniea, K., Rugela, G., Wallnerd, A., Dillmanna, I., Dollingerb, G., Lierse von Gostomskie, Ch, Kossertf, K., Maitia, M., Poutivtseva, M., Remmer, A., 2010. A new value for the half-life of ^{10}Be by heavy ion elastic recoil detection and liquid scintillation counting. Nucl. Instrum. Methods Phys. Res. B 268, 187–191.
Krabbendam, M., Bradwell, T., 2014. Quaternary evolution of glaciated gneiss terrains: pre-glacial weathering vs. glacial erosion. Quat. Sci. Rev. 95, 20–42.
Lal, D., 1991. Cosmic ray labeling of erosion surfaces: in situ nuclide production rates and erosion models. Earth Planet. Sci. Lett. 104, 424–439.
Li, Y.K., Harbor, J., Stroeven, A.P., Fabel, D., Kleman, J., Fink, D., Caffee, M., Elmore, D., 2005. Ice Sheet erosion patterns in valley systems in northern Sweden investigated using cosmogenic nuclides. Earth Surf. Process. Landforms 30, 1039–1049.
Linge, H., Brook, E.J., Nesje, A., Raisbeck, G.M., Yiou, F., Clark, H., 2006. In situ 10Be exposure ages from southeastern Norway: implications for the geometry of the Weichselian Scandinavian ice sheet. Quat. Sci. Rev. 25, 1097–1109.
Lidmar-Bergström, K., 1996. Long term morphotectonic evolution in Sweden. Geomorphology 16, 33–59.
Lisiecki, L.E., Raymo, M.E., 2005. A Pliocene-Pleistocene stack of 57 globally distributed benthic δ^{18}O records. Paleoceanography 20, PA1003.
Mangerud, J., Gyllencreutz, R., Lohne, Ø.S., Svendsen, J.I., 2011. Glacial history of Norway. In: Ehlers, J., Gibbard, P.L., Hughes, P.D. (Eds.), Developments in Quaternary Science, vol. 15, pp. 279–298.
Margreth, A., Gosse, J., Dyke, A., 2016. Quantification of subaerial and episodic subglacial erosion rates on high latitude upland plateaus: cumberland Peninsula, Baffin Island, Arctic Canada. Quat. Sci. Rev. 133, 108–129.
Medvedev, S., Hartz, E.H., 2015. Evolution of topography of post-Devonian Scandinavia: effects and rates of erosion. Geomorphology 231, 229–245.
Nesje, A., Dahl, S.O., Valen, V., Øvstedal, J., 1992. Quaternary erosion in the Sognefjord drainage basin, western Norway. Geomorphology 5, 511–520.
Nielsen, S.B., Gallagher, K., Leighton, C., Balling, N., Svenningsen, L., Jacobsen, B.H., Thomsen, E., Nielsen, O.B., Heilmann-Clausen, C., Egholm, D.L., Summerfield, M.A., Clausen, O.R., Piotrowski, J.A., Thorsen, M.R., Huuse, M., Abrahamsen, N., King, C., Lykke Andersen, H., 2009. The evolution of western Scandinavian topography: a review of Neogene uplift versus the ICE (isostasy–climate–erosion) hypothesis. J. Geodyn. 47, 72–95.
Nishiizumi, K., Kohl, C.P., Arnold, J.R., Klein, J., Fink, D., Middleton, R., 1991. Cosmic ray produced ^{10}Be and ^{26}Al in Antarctic rocks: exposure and erosion history. Earth Planet. Sci. Lett. 104, 440–454.
Nishiizumi, K., 2004. Preparation of ^{26}Al AMS standards. Nucl. Instrum. Methods Phys. Res. B 223–224, 388–392.
Olesen, O., Bering, D., Brönner, M., Dalsegg, E., Fabian, K., Fredin, O., Gellein, J., Berit Husteli, B., Magnus, C., Rønning, J.S., Solbakk, T., Tønnesen, J.F., Øverland, J.A., 2012. Tropical Weathering in Norway. Geological Survey of Norway. Report 2012.005, 188 pp.
Paasche, Ø., Strømsøe, J.R., Dahl, S.O., Linge, H., 2006. Weathering characteristics of arctic islands in northern Norway. Geomorphology 82, 430–452.
Refsnider, K.A., Miller, G.H., 2010. Reorganization of ice sheet flow patterns in Arctic Canada and the Mid-Pleistocene Transition. Geophys. Res. Lett. 37, L13502.
Refsnider, K.A., Miller, G.H., 2013. Ice-sheet erosion and the stripping of tertiary regolith from Baffin island, eastern Canadian arctic. Quat. Sci. Rev. 67, 176–189.
Reiners, P.W., Brandon, M.T., 2006. Using thermochronology to understand orogenic erosion. Annu. Rev. Earth Planet Sci. 34, 419–466.
Reusch, H., 1901. Nogle bidrag til forstaaelsen af hvorledes Norges dale og fjelde er blevne til. Norges Geologiske Undersøkelse 32 (124–217), 239–263 (in Swedish).
Reusch, H., 1910. A few words on the effects of glacial erosion in Norway. In: Extrait du Compte Rendu du XI:e Congrès Géologique International.
Richter, E., 1896. Geomorphologische Beobachtungen aus Norwegen. In: Sitzungsberichte der Kaiserlichen Akademie der Wissenschaften Mathematisch-Naturwissenschaftliche Klasse, vol. 105, pp. 147–189 (in German).
Rudberg, S., 1954. Västerbottens berggrundsmorfologi. In: Ett Försök till Rekonstruktion Av Preglaciala Erosionsgenerationer I Sverige Geographica, vol. 25, 457 pp. Uppsala (in Swedish).
Steer, P., Huismans, R.S., Valla, P.G., Gac, S., Herman, F., 2012. Bimodal Plio-Quaternary glacial erosion of fjords and low-relief surfaces in Scandinavia. Nat. Geosci. 5, 635–639.
Stone, J., 2000. Air pressure and cosmogenic isotope production. J. Geophys. Res. 105, 23753–23760.
Stroeven, A.P., Fabel, D., Hättestrand, C., Harbor, J., 2002. A relict landscape in the centre of Fennoscandian glaciation; cosmogenic radionuclide evidence of tors preserved through multiple glacial cycles. Geomorphology 44, 145–154.
Stroeven, A.P., Hättestrand, C., Kleman, J., Heyman, J., Fabel, D., Fredin, O., Goodfellow, B.W., Harbor, J.M., Jansen, J.D., Olsen, L., Caffee, M.W., Fink, D., Lundqvist, J., Rosqvist, G.C., Strömberg, B., Jansson, K.N., 2016. Deglaciation of Fennoscandia. Quat. Sci. Rev. 147, 91–121.
Strunk, A., Knudsen, M.K., Egholm, D.L., Jansen, J.D., Levy, L.B., Jacobsen, B.H., Larsen, N.K., 2017. One million years of glaciation and denudation history in west Greenland. Nat. Commun. 8, 14199.
Strømsøe, J.R., Paasche, Ø., 2011. Weathering patterns in high-latitude regolith. J. Geophys. Res. 116, F03021.
Sugden, D.E., 1974. Landscapes of glacial erosion in Greenland and their relationship to ice, topographic and bedrock conditions. In: Brown, E.H., Waters, R.S. (Eds.), Progress in Geomorphology, vol. 7. Institute of British Geographers Special Publication, pp. 177–195.
Sugden, D.E., 1978. Glacial erosion by the Laurentide ice sheet. J. Glaciol. 20, 367–391.
Sugden, D.E., John, B.S., 1976. Glaciers and Landscape: a Geomorphological Approach. Arnold, London.
Sugden, D., Watts, S., 1977. Tors, felsenmeer, and glaciation in northern cumberland Peninsula, Baffin island. Can. J. Earth Sci. 14, 2817–2823.
White, W.A., 1988. More on deep glacial erosion by continental ice sheets and their tongues of distributary ice. Quat. Res. 30, 137–150.
Young, N.E., Briner, J.P., Maurer, J., Schaefer, J.M., 2016. ^{10}Be measurements in bedrock constrain erosion beneath the Greenland Ice Sheet margin. Geophys. Res. Lett. 43 (11), 708–711, 719.
Zachos, J., Pagani, M., Sloan, L., Thomas, E., Billups, K., 2001. Trends, rhythms, and aberrations in global climates 65 Ma to present. Science 292, 686–693.